Computational understanding of the band alignment engineering in PbI$_2$/PtS$_2$ heterostructure: Effects of electric field and vertical strain

P.T.T. Le [a,b], Doan V. Thuan [c], Huynh V. Phuc [d], Nguyen N. Hieu [e], H.D. Bui [e,**], Bin Amin [f], Chuong V. Nguyen [g,*]

[a] Laboratory of Magnetism and Magnetic Materials, Advanced Institute of Materials Science, Ton Duc Thang University, Ho Chi Minh City, Vietnam
[b] Faculty of Applied Sciences, Ton Duc Thang University, Ho Chi Minh City, Vietnam
[c] NTT Hi-Tech Institute, Nguyen Tat Thanh University, Ho Chi Minh City, Vietnam
[d] Division of Theoretical Physics, Dong Thap University, Cao Lanh, Vietnam
[e] Institute of Research and Development, Duy Tan University, Da Nang 550000, Vietnam
[f] Department of Physics, Abbottabad University of Science and Technology, Abbottabad 22010, Pakistan
[g] Department of Materials Science and Engineering, Le Quy Don Technical University, Ha Noi, Vietnam

ABSTRACT

In this work, a new type of two-dimensional-based heterostructure PbI$_2$/PtS$_2$ has been constructed for the first time and its electronic properties and band alignment have been investigated systematically through first-principles calculations. Our results show that at the ground state, the PbI$_2$/PtS$_2$ heterostructure is mainly characterized by a weak vdW interaction. Moreover, such heterostructure forms a type-II band alignment and shows a semiconducting character with an indirect band gap of 1.90 eV. The band alignment in the PbI$_2$/PtS$_2$ heterostructure can be controlled under the application of the electric field and vertical strain, which can result on the semiconductor to metal transition. These findings provide an effective approach for designing new electronic and optoelectronic nanodevices based on PbI$_2$/PtS$_2$ heterostructure.

1. Introduction

Owing to their superior properties, two-dimensional materials (2D) have been considered as the promising materials that can be widely used in high-speed electronic nanodevices [1–4]. To the best of our knowledge, among these 2D materials, 2D MoS$_2$ crystal is one of the most considered material for device applications [5–7]. Different from semi-metallic graphene, MoS$_2$ monolayer has been demonstrated to be a semiconductor, that makes it desirable material for high-speed electronic nanodevices [6]. Due to a high carrier mobility of MoS$_2$ monolayer, Rdisavljevic et al. demonstrated that it can be used to fabricate a transistor with a high on/off ratios at room temperature [5]. Thus, seeking for new materials with desirable properties for the design and fabrication of the next-generation electronic nanodevices is currently attracting considerable interest in the research community.

Looking beyond this field, single-layers of lead iodide (PbI$_2$) and platinum disulfide (PtS$_2$) have recently been extensively studied both experimentally and theoretically. The PbI$_2$ monolayer is found to have an indirect band gap semiconductor and it can be obtained in experiment via hydrothermal method [8] or physical vapour deposition (PVD) [9]. Whereas, the PtS$_2$ monolayer is known as an indirect band gap semiconductor with high carrier mobility of 1107 cm^2/V [10]. Both the PbI$_2$ and PtS$_2$ monolayers have been demonstrated to be potential candidates for next-generation electronic nanodevices, such as light-emitting field-effect transistor [11], solar cell [10,12].

Currently, one of the most effective approach, which can be used widely to break the limitations and to extend the application possibilities of single layer 2D materials, that is to construct their layered van der Waals (vdW) heterostructure (HS) [13–15]. To now, the vdW HS based on different 2D single layered materials can be synthesized easily in experiment via various common methods, such as chemical vapour deposition (CVD) [16–18], mechanical exfoliation [19,20] and so forth. Up to now, many vdW HS based on 2D materials have been proposed theoretically and fabricated experimentally, such as graphene-based HS [21–26], phosphorene-based HS [27–30], arsenene-based HS [31–33] and so on. One can find that these HS shows many interesting properties,

---
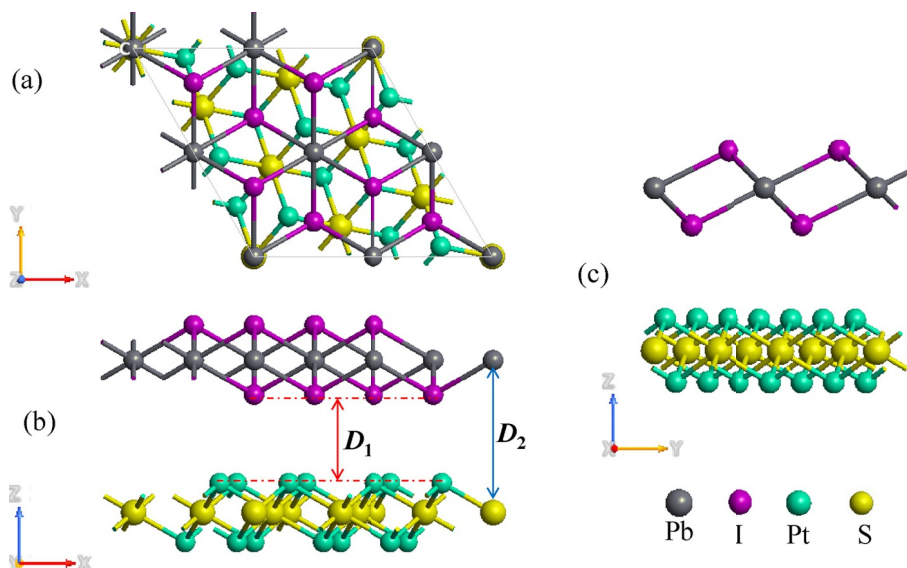
Fig. 1. (a) Top view, (b, c) side views of the PbI_2/PtS_2 HS after geometric optimization. D_1 and D_2 stand for the interlayer distances in the heterostructure.

that do not exist in single layered 2D materials. To date, there exists a few research studies that have been focused on the vdW HS based on the PbI_2 monolayer, such as PbI_2/BN [34], PbI_2/MoS_2 [35], $PbI_2/phos-phorene$ [36] and on the PtS_2 monolayer, such as $PtS_2/InSe$ [37]. However, to the best of our knowledge, up to date, there is no literature about the combination between the PbI_2 and the PtS_2 monolayers. Thus, we have a bold idea to construct a new PbI_2/PtS_2 HS and then investigate its electronic properties and band alignment engineering through DFT calculations.

2. Computational methodology

All the calculations in this work, including geometric optimization and electronic properties calculations were carried out through density functional theory (DFT) from the Quantum Espresso code [38]. The projector-augmented wave (PAW) method through the Predew-Burke-Ernzerhof (PBE) functional within the generalized gradient approximation (GGA) formalism were applied to describe electron-ion interactions and the exchange-correlation potentials. A plane wave basis set with a cut-off energy of 500 eV and a $6 \times 6 \times 1$ k-points grid in the Brillouin zone were used. Gaussian smearing was used to determine the partial occupancies for each orbital with the smearing width of 0.05 eV by convergence test. The atomic structures

were relaxed using conjugate gradient algorithm as implemented in the Quantum Espresso code until the forces on all unconstrained atoms were smaller than 0.01 eV/Å. A vacuum region of 20 Å along the z direction was used to separate the two heterostructures in order to avoid spurious interaction due to the nonlocal nature of the correlation energy. The corrected dispersion DFT-D2 method of Grimme [39] is used to account for long range vdW interaction between monolayers PtS_2 and PbI_2. Moreover, in order to obtain an accurate description of atoms containing d-electrons, such as Pt and Pb atoms, we used a finite on-site Coulomb interaction by using the GGA + U method for describing the 3d transition metal atoms. We adopt an onsite Coulomb interaction of U = 4.0 eV for Pt and U = 8.5 eV for Pb atoms, respectively.

3. Results and discussion

Firstly, it shown be noted that monolayers of different types have different lattice constants. Thus, to study heterostructures ones need to construct supercells. One such supercell contains several cells of each monolayer. That makes the problem much more complicated. Before constructing the HS from PbI_2 and PtS_2 monolayers, it is necessary to check the lattice parameters of the single layered 2D materials. Our calculated lattice parameters of perfect PbI_2 and PtS_2 monolayers, respectively, are 4.68 Å and 3.54 Å, indicating a large lattice mismatch
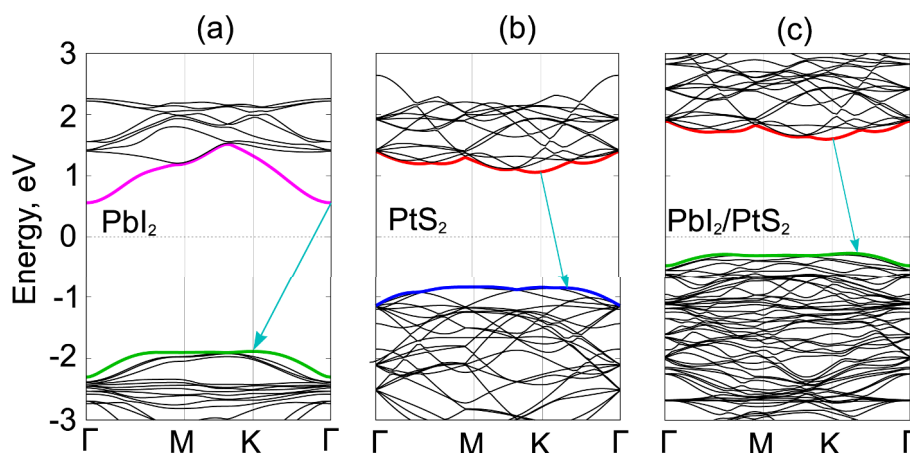
**Fig. 2.** Calculated band structures of single layers of (a) PbI_2 monolayer (b) PtS_2 monolayer, and (c) their PbI_2/PtS_2 HS.
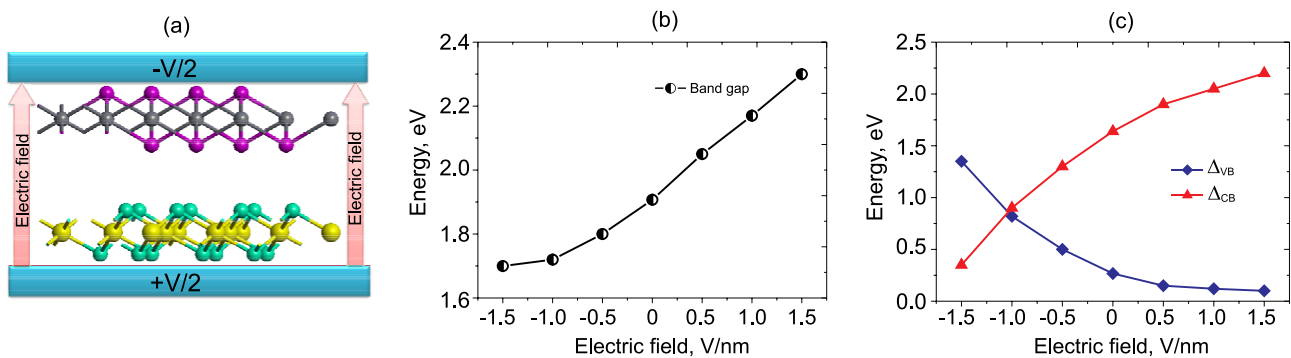
Fig. 3. (a) Schematic model of electric field, applied to the PbI$_2$/PtS$_2$ HS along the z direction. The evolution of the band gap (b) and the positions of the CBM and VBM, related to the Fermi level of the PbI$_2$/PtS$_2$ HS as a function of electric field.

of about 23%. It should be noted that the accuracy of the lattice parameter of PbI$_2$ and PtS$_2$ monolayers strongly depends on the k point mesh and cut-off energy. Thus, before constructing the heterostructure, we calculate the accuracy of the obtained results, as presented in Fig. S1 (see ESI). To minimize this large mismatch, we use a supercell with (2×2) PbI$_2$ supercell and $(2\sqrt{2} \times 2\sqrt{2})$ PtS$_2$ supercell. The overall lattice mismatch between two different monolayers in the HS is about 3%. The most stable stacking configuration of the PbI$_2$/PtS$_2$ HS is presented in Fig. 1. We then perform a full geometric optimization process and obtain the equilibrium interlayer distance D_1 and D_2, which are 3.27 Å and 6.423 Å, respectively. Compared to that in other 2D heterostructures, which are typical vdW interactions, such as graphene/GaN [24] ($D_1 = 3.28$ Å), MoS$_2$/SnS$_2$ [40] ($D_1 = 3.32$ Å), graphene/SnS [41] ($D_1 = 3.32$ Å) etc, we can find that the interlayer distance in PbI$_2$/PtS$_2$ HS has the same order of magnitude. In addition, one can observe that D_1 is quite smaller that the sum of the vdW radii of interfacial S (1.80 Å) and I (1.98 Å) atoms. This suggests that the S and I layers are displaced

and the atoms are not strictly on top of each other. Thus, we can conclude that the PbI$_2$/PtS$_2$ HS is a typical vdW system.

The binding energy (E_b) is also established in order to evaluate the structural stability of the PbI$_2$/PtS$_2$ HS. E_b can be determined as $E_b = [E_{HS} - E_{PbI_2} - E_{PtS_2}]/N$, where E_{HS}, E_{PbI_2}, and E_{PtS_2} are the total energies of the HS, isolated PbI$_2$ and PtS$_2$ monolayers, respectively. N = 2 stands for the number of PbI$_2$ unit cells in the HS. The binding energy per PbI$_2$ unit cell is calculated to be $E_b = -0.59$ eV. Such E_b value is more negative than that of previously typical vdW HS, such as MoS$_2$/PbI$_2$ [35] ($E_b = -0.234$ eV per MoS$_2$ unit cell), phophorene/PbI$_2$ [36] ($E_b = -0.476$ eV per phosphorene unit cell). The greater the binding energy is, the more stable the heterostructure becomes. Hence, our considered here heterostructures will be comparatively very stable. Also, this could be just more evidence for that the interaction between PbI$_2$ and PtS$_2$ monolayers in their heterostructures is mainly forced through vdW interactions.

Now, we change to calculate the band structures of the isolated PbI$_2$
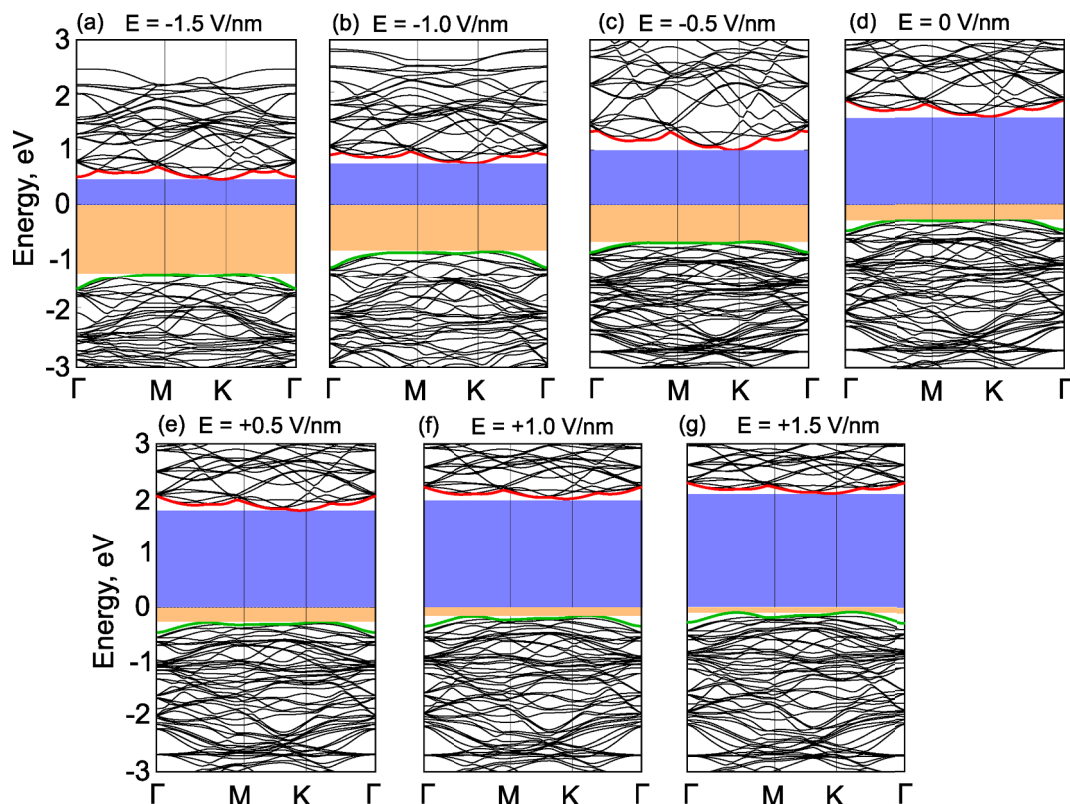
Fig. 4. Calculated electronic band structures of PbI$_2$/PtS$_2$ HS under different strengths of electric field $E_\perp$: (a) $E_\perp = -1.5$ V/nm, (b) $E_\perp = -1.0$ V/nm, (c) $E_\perp = -0.5$ V/nm, (d) $E_\perp = 0$ V/nm, (e) $E_\perp = +0.5$ V/nm, (f) $E_\perp = +1.0$ V/nm, (g) $E_\perp = +1.5$ V/nm. The Fermi level is defined by the dashed line and is set to be zero.
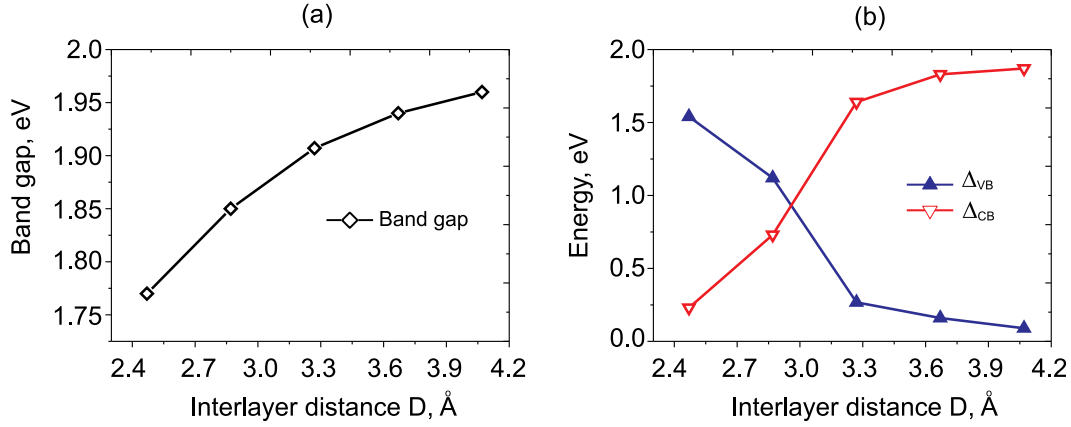
Fig. 5. The evolution of the band gap (a) and the band edge positions (b) of the PbI$_2$/PtS$_2$ HS as a function of the vertical strain.

and PtS$_2$ monolayers as well as their PbI$_2$/PtS$_2$ HS at the equilibrium state. These band structures are presented in Fig. 2. The calculated indirect band gap of the isolated PbI$_2$ and PtS$_2$ monolayer, as illustrated in Fig. 2(a) and (b), respectively are 2.44 eV and 1.95 eV. The band structure of PbI$_2$/PtS$_2$ HS is illustrated in Fig. 2(c). It shows a semiconducting character with an indirect band gap of 1.90 eV. It is clear that such band gap of HS is smaller than that of the parent 2D materials. The conduction band minimum (CBM) of PbI$_2$/PtS$_2$ HS comes from the CBM of PtS$_2$ monolayer, whereas its valence band maximum (VBM) comes from the VBM of PbI$_2$ monolayer. This indicates a type-II staggered-gap band alignment in PbI$_2$/PtS$_2$ HS.

It is interesting that the electric field and strains can tune the electronic properties of the heterostructures, the device performance thus can be also enhanced. Therefore, in order to extend the range of application of 2D materials based heterostructures, we further investigate the effects of the electric field and strain on the electronic properties of heterostructure. The electric field is applied along the z direction of the heterostructure, as illustrated in Fig. 3(a). The change in the band gap of HS under different strengths of the positive and negative electric fields is displayed in Fig. 3(b). The band gap increases from 1.70 eV to 2.30 eV with increasing electric field from −1.5 V/nm to +1.5 V/nm, respectively. The nature of this change can be described via the position of the VBM and CBM, related to the Fermi level and the band structures of such HS under different strengths of electric fields. Thus, in Figs. 3(c) and 4 we plot the position of the VBM and CBM, related to the Fermi level of such HS as well as its band structures under different strengths of electric fields. The difference in energy between the VBM/CBM and the Fermi level is calculated as $\Delta_{VB} = E_F$ - $E_{VBM}/\Delta_{CB} = E_{CBM}$ - E_F. We can see that with increasing electric field from −1.5 V/nm to +1.5 V/nm the Δ_{CB} increases, whereas the Δ_{VB} decreases, as presented in Fig. 3(c). Interestingly, an increment of the Δ_{CB} is larger than a decrement of the Δ_{VB}

when the electric field is applied. The band gap of the PbI$_2$/PtS$_2$ HS, therefore, increases with increasing electric field from −1.5 V/nm to +1.5 V/nm. By analyzing the band structures of the PbI$_2$/PtS$_2$ HS as presented in Fig. 4, one can see that applying negative electric field tends to the shift of the Fermi level from the VBM towards the CBM of the PbI$_2$/PtS$_2$ HS. On the other hand, applying positive electric field leads to the downshifting of the Fermi level from the CBM toward the VBM. Interestingly, our calculations demonstrates that the transition from semiconductor to metal can be achieved in the PbI$_2$/PtS$_2$ HS when the positive electric field is larger than +2 V/nm.

The effects of vertical strain on the band gap and band edge positions of the PbI$_2$/PtS$_2$ HS are presented in Fig. 5. It is clear that the vertical strain can modulate both the band gap and band edge positions of such heterostructure. And indeed, we can see from Fig. 5(a) that the band gap increases gradually with increasing interlayer distance D from 2.47 Å to 4.07 Å. Like the band gap, the band edge positions of the PbI$_2$/PtS$_2$ HS also change when the vertical strain is tuned. The Δ_{VB} reduces when we increase the interlayer distance D, whereas the Δ_{CB} increases. Our calculations demonstrate that the Δ_{VB} can reduce to zero when the interlayer distance is larger than 4.2 Å. It indicates that the transition from the semiconductor to metal can be achieved with increasing the interlayer distance. The change in the band gap and band edge positions of the PbI$_2$/PtS$_2$ HS can be explained by analyzing its band structures at the different interlayer distances, as displayed in Fig. 6. Indeed, we find that when the interlayer distance is reduced from 3.27 Å to 2.47 Å, the Fermi level of the PbI$_2$/PtS$_2$ HS is upshifted from the VBM toward the CBM. On the contrary, when the interlayer distance D increases from 3.27 Å to 4.07 Å, the Fermi level of the PbI$_2$/PtS$_2$ HS tends to the downshifting from its CBM toward the VBM, leading to the increase/decrease in the Δ_{CB}/Δ_{VB}. Therefore, we can conclude that the vertical strain can be used to tune effectively the band gap and band edge positions of the PbI$_2$/PtS$_2$
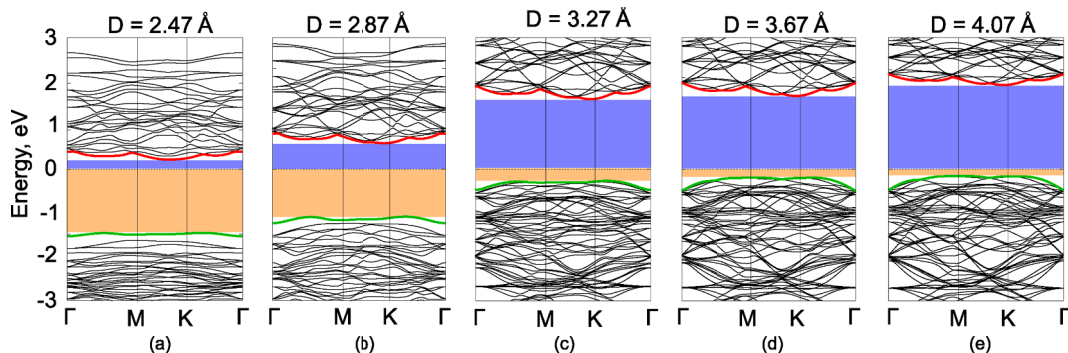

Fig. 6. Calculated electronic band structures of PbI$_2$/PtS$_2$ HS under different interlayer distances D: (a) $D = 2.47$ Å, (b) $D = 2.87$ Å, (c) $D = 3.27$ Å, (d) $D = 3.67$ Å, (e) $D = 4.07$ Å. The Fermi level is defined by the dashed line and is set to be zero.

HS.

4. Conclusion

In conclusion, we have designed the PbI_2/PtS_2 HS and investigated its structural and electronic properties as well as the effects of electric field and vertical strain using DFT calculations. At the ground state, the PbI_2/PtS_2 HS is mainly characterized by a weak vdW interaction. Moreover, it exhibits a type-II band alignment and shows a semiconducting character with an indirect band gap of 1.90 eV. The band alignment in the PbI_2/PtS_2 HS can be controlled when it subjected to the external conditions, including electric field and vertical strain. Our results demonstrates that the external electric fields and vertical strains are efficient to tune the band gap and band edge positions of the PbI_2/PtS_2 HS, which can result on the semiconductor to metal transition. These results may provide potential guidance towards PbI_2/PtS_2 HS-based electronic and optoelectronic nanodevices.

Conflicts of interest

There are no conflicts to declare.

Acknowledgements

Appendix A. Supplementary data

Supplementary data to this article can be found online at https://doi.org/10.1016/j.physe.2019.113706.

References

[1] A. Neto, K. Novoselov, Mater. Exp. 1 (1) (2011) 10–17.
[2] M. Xu, T. Liang, M. Shi, H. Chen, Chem. Rev. 113 (5) (2013) 3766–3798.
[3] S.Z. Butler, S.M. Hollen, L. Cao, Y. Cui, J.A. Gupta, H.R. Gutiérrez, T.F. Heinz, S. S. Hong, J. Huang, A.F. Ismach, et al., ACS Nano 7 (4) (2013) 2898–2926.
[4] G. Fiori, F. Bonaccorso, G. Iannaccone, T. Palacios, D. Neumaier, A. Seabaugh, S. K. Banerjee, L. Colombo, Nat. Nanotechnol. 9 (10) (2014) 768.
[5] B. Radisavljevic, A. Radenovic, J. Brivio, i.V. Giacometti, A. Kis, Nat. Nanotechnol. 6 (3) (2011) 147.
[6] Y. Yoon, K. Ganapathi, S. Salahuddin, Nano Lett. 11 (9) (2011) 3768–3773.
[7] W. Zhang, J.-K. Huang, C.-H. Chen, Y.-H. Chang, Y.-J. Cheng, L.-J. Li, Adv. Mater. 25 (25) (2013) 3456–3461.
[8] X. Zhu, P. Wangyang, H. Sun, D. Yang, X. Gao, H. Tian, Mater. Lett. 180 (2016) 59–62.
[9] M. Zhong, S. Zhang, L. Huang, J. You, Z. Wei, X. Liu, J. Li, Nanoscale 9 (11) (2017) 3736–3741.
[10] Y. Zhao, J. Qiao, P. Yu, Z. Hu, Z. Lin, S.P. Lau, Z. Liu, W. Ji, Y. Chai, Adv. Mater. 28 (12) (2016) 2399–2407.
[11] X.Y. Chin, D. Cortecchia, J. Yin, A. Bruno, C. Soci, Nat. Commun. 6 (2015) 7383.
[12] F. Liu, Q. Dong, M.K. Wong, A.B. Djurišić, A. Ng, Z. Ren, Q. Shen, C. Surya, W. K. Chan, J. Wang, A.M.C. Ng, C. Liao, H. Li, K. Shih, C. Wei, H. Su, J. Dai, Adv. Energy Mater. 6 (7) (2016) 1502206.
[13] A.K. Geim, I.V. Grigorieva, Nature 499 (7459) (2013) 419.
[14] K. Novoselov, A. Mishchenko, A. Carvalho, A.C. Neto, Science 353 (6298) (2016) aac9439.
[15] Y. Liu, N.O. Weiss, X. Duan, H.-C. Cheng, Y. Huang, X. Duan, Nat. Rev. Mater. 1 (9) (2016) 16042.
[16] S. Wang, X. Wang, J.H. Warner, ACS Nano 9 (5) (2015) 5246–5254.
[17] Q.H. Wang, K. Kalantar-Zadeh, A. Kis, J.N. Coleman, M.S. Strano, Nat. Nanotechnol. 7 (11) (2012) 699.
[18] M.-Y. Li, C.-H. Chen, Y. Shi, L.-J. Li, Mater. Today 19 (6) (2016) 322–335.
[19] H. Sediri, D. Pierucci, M. Hajlaoui, H. Henck, G. Patriarche, Y.J. Dappe, S. Yuan, B. Toury, R. Belkhou, M.G. Silly, et al., Sci. Rep. 5 (2015) 16465.
[20] D. Pierucci, H. Henck, J. Avila, A. Balan, C.H. Naylor, G. Patriarche, Y.J. Dappe, M. G. Silly, F. Sirotti, A.T.C. Johnson, M.C. Asensio, A. Ouerghi, Nano Lett. 16 (7) (2016) 4054–4061.
[21] H. Henck, Z. Ben Aziza, D. Pierucci, F. Laourine, F. Reale, P. Palczynski, J. Chaste, M.G. Silly, F.m. c. Bertran, P. Le Fèvre, E. Lhuillier, T. Wakamura, C. Mattevi, J. E. Rault, M. Calandra, A. Ouerghi, Phys. Rev. B 97 (2018) 155421.
[22] Z. Ben Aziza, D. Pierucci, H. Henck, M.G. Silly, C. David, M. Yoon, F. Sirotti, K. Xiao, M. Eddrief, J.-C. Girard, A. Ouerghi, Phys. Rev. B 96 (2017) 035407.
[23] M. Sun, J.-P. Chou, J. Yu, W. Tang, Phys. Chem. Chem. Phys. 19 (26) (2017) 17324–17330.
[24] M. Sun, J.-P. Chou, Q. Ren, Y. Zhao, J. Yu, W. Tang, Appl. Phys. Lett. 110 (17) (2017) 173105.
[25] K.D. Pham, N.N. Hieu, V.V. Ilyasov, H.V. Phuc, B.D. Hoi, E. Feddi, N.V. Thuan, C. V. Nguyen, Superlattice Microstruct. 122 (2018) 570–576.
[26] C.V. Nguyen, Superlattice Microstruct. 116 (2018) 79–87.
[27] Q. Peng, Z. Wang, B. Sa, B. Wu, Z. Sun, Sci. Rep. 6 (2016) 31994.
[28] W. Yu, Z. Zhu, S. Zhang, X. Cai, X. Wang, C.-Y. Niu, W.-B. Zhang, Appl. Phys. Lett. 109 (10) (2016) 103104.
[29] Z. Guo, N. Miao, J. Zhou, B. Sa, Z. Sun, J. Mater. Chem. C 5 (4) (2017) 978–984.
[30] V.D.S. Ganesan, J. Linghu, C. Zhang, Y.P. Feng, L. Shen, Appl. Phys. Lett. 108 (12) (2016) 122105.
[31] X.-H. Li, B.-J. Wang, X.-L. Cai, L.-W. Zhang, G.-D. Wang, S.-H. Ke, RSC Adv. 7 (45) (2017) 28393–28398.
[32] H. Zeng, J. Zhao, A.-Q. Cheng, L. Zhang, Z. He, R.-S. Chen, Nanotechnology 29 (7) (2018) 075201.
[33] F. Zhang, W. Li, X. Dai, Superlattice Microstruct. 104 (2017) 518–524.
[34] Y. Ma, X. Zhao, M. Niu, X. Dai, W. Li, X. Wang, M. Zhao, T. Wang, Y. Tang, Appl. Surf. Sci. 411 (2017) 46–52.
[35] Y. Ma, X. Zhao, T. Wang, W. Li, X. Wang, S. Chang, Y. Li, M. Zhao, X. Dai, Phys. Chem. Chem. Phys. 18 (41) (2016) 28466–28473.
[36] Y. Wei, F. Wang, W. Zhang, X. Zhang, Phys. Chem. Chem. Phys. 21 (2019) 7765–7772.
[37] C.V. Nguyen, H. Bui, T.D. Nguyen, K.D. Pham, Chem. Phys. Lett. 724 (2019) 1–7.
[38] P. Giannozzi, S. Baroni, N. Bonini, M. Calandra, R. Car, C. Cavazzoni, D. Ceresoli, G.L. Chiarotti, M. Cococcioni, I. Dabo, A.D. Corso, S. de Gironcoli, S. Fabris, G. Fratesi, R. Gebauer, U. Gerstmann, C. Gougoussis, A. Kokalj, M. Lazzeri, L. Martin-Samos, N. Marzari, F. Mauri, R. Mazzarello, S. Paolini, A. Pasquarello, L. Paulatto, C. Sbraccia, S. Scandolo, G. Sclauzero, A.P. Seitsonen, A. Smogunov, P. Umari, R.M. Wentzcovitch, J. Phys. Condens. Matter 21 (2009) 395502–395520.
[39] S. Grimme, J. Comput. Chem. 27 (2006) 1787–1799.
[40] D.S. Koda, F. Bechstedt, M. Marques, L.K. Teles, Phys. Rev. B 97 (16) (2018) 165402.
[41] W. Xiong, C. Xia, X. Zhao, T. Wang, Y. Jia, Carbon 109 (2016) 737–746.